Journal of Materials Chemistry C

PAPER

View Article Online
View Journal | View Issue

Published on 09 September 2016. Downloaded by Synchrotron Radiation Library on 11/09/2017 07:30:03.

Cite this: J. Mater. Chem. C, 2016, 4, 9266

Highly planar cross-conjugated alternating polymers with multiple conformational locks: synthesis, characterization and their field-effect properties†

Weifeng Zhang,‡[a] Zupan Mao,‡[a] Naihang Zheng,[a] Jiabin Zou,[b] Liping Wang,*[b] Congyuan Wei,[a] Jianyao Huang,[a] Dong Gao[a] and Gui Yu*[ac]

Received 9th July 2016,
Accepted 9th September 2016

DOI: 10.1039/c6tc02891h

www.rsc.org/MaterialsC

It is meaningful to explore new design principles for organic semiconductors. Herein, we have developed two cross-conjugated alternating polymers based on 1,2-di(thiophen-2-yl)ethane-1,2-dione (DTO), namely PDTO-C1 and PDTO-C3, and investigated their charge transport properties by fabricating field-effect transistors devices. Single crystal X-ray crystallography shows that non-covalent S···O and C–H···O interactions exist inside the DTO units. These non-covalent interactions in combination with the C–H···O interactions of the thiophene-flanked dithienothiophene units, acting as conformational locks, are beneficial for acquiring the planar backbone conformation. PDTO-C1 and PDTO-C3 possess broad absorption spectra and HOMO and LUMO energy levels of *ca.* −5.50 and −3.6 eV, respectively. The highest mobility of 0.54 $cm^2\ V^{-1}\ s^{-1}$ was achieved in the PDTO-C3-based transistor devices, whereas PDTO-C1 affords a mobility of 0.22 $cm^2\ V^{-1}\ s^{-1}$. Further thin film microstructure investigations indicate that both polymers can form highly-ordered lamellar packing with small π–π stacking distances down to 3.50 Å. These results demonstrate that the incorporation of cross-conjugation may be used as an additional design tactic for organic semiconductors to alter their optoelectronic properties.

Introduction

Solution-processable semiconducting polymers have attained a lot of attention due to their great potential in fabricating large-area, flexible light-emitting diodes,[1–3] organic field-effect transistors (OFETs)[4–7] and organic photovoltaics,[8–12] through widely used fast printing techniques. Depending on a successful donor–acceptor (D–A) approach along with general design strategies such as the reduction of the backbone conformation twists and regulation of the frontier orbital energy levels (HOMO and LUMO), specialized semiconducting polymers for these electronic devices have been developed, each with the optoelectronic properties tuned to the respective specific requirements. Almost all of the studies currently concern semiconducting polymers with linearly π-conjugated systems.[13,14] However, systems with cross-conjugated π-systems have seldom been touched though cross-conjugation can be found in a wide range of small molecules, including such examples as radialenes, quinones and fulvalenes.[15] Therefore, developing semiconducting polymers with cross-conjugated structures and investigating their field-effect properties would be an interesting exploration.

Linear conjugation has alternating single and double bonds, broken conjugation has conjugation-break spacers along the conjugated backbone and cross-conjugation means the structure has three unsaturated groups, two of which although conjugated to a third unsaturated centre are not conjugated to each other. The three conjugation patterns are schematically illustrated using vinyl compounds as examples and the thiophene-based units such as (*E*)-1,2-di(thiophen-2-yl)ethene (**DTE**), 1,2-di(thiophen-2-yl)ethane (**TC2T**) and di(thiophen-2-yl)ethane-1,2-dione (**DTO**) as shown in Fig. 1a. Linearly π-conjugated D–A polymers often possess weakly polarized states along their conjugated skeleton, which will promote the charge injection at the electrode/semiconductor interface and facilitate charge transport in the polymer active layers.[16,17] The current state-of-the-art charge carrier mobility of linearly conjugated D–A polymers is close to or exceeding 10 $cm^2\ V^{-1}\ s^{-1}$ for both p- and n-channel operations, which is comparable to the amorphous silicon-based FETs.[6–9] Nevertheless, D–A polymers with an alkyl-derived broken spacer only afford

[a] Beijing National Laboratory for Molecular Sciences, Institute of Chemistry, Chinese Academy of Sciences, Beijing 100190, P. R. China. E-mail: yugui@iccas.ac.cn
[b] School of Material Science and Engineering, University of Science and Technology Beijing, Beijing 100083, P. R. China. E-mail: lpwang@mater.ustb.edu.cn
[c] University of Chinese Academy of Sciences, Beijing 100049, P. R. China

† Electronic supplementary information (ESI) available. CCDC 1400329. For ESI and crystallographic data in CIF or other electronic format see DOI: 10.1039/c6tc02891h

‡ The authors W. F. Zhang and Z. P. Mao contributed equally to this work.

This journal is © The Royal Society of Chemistry 2016

Published on 09 September 2016. Downloaded by Synchrotron Radiation Library on 11/09/2017 07:30:03.

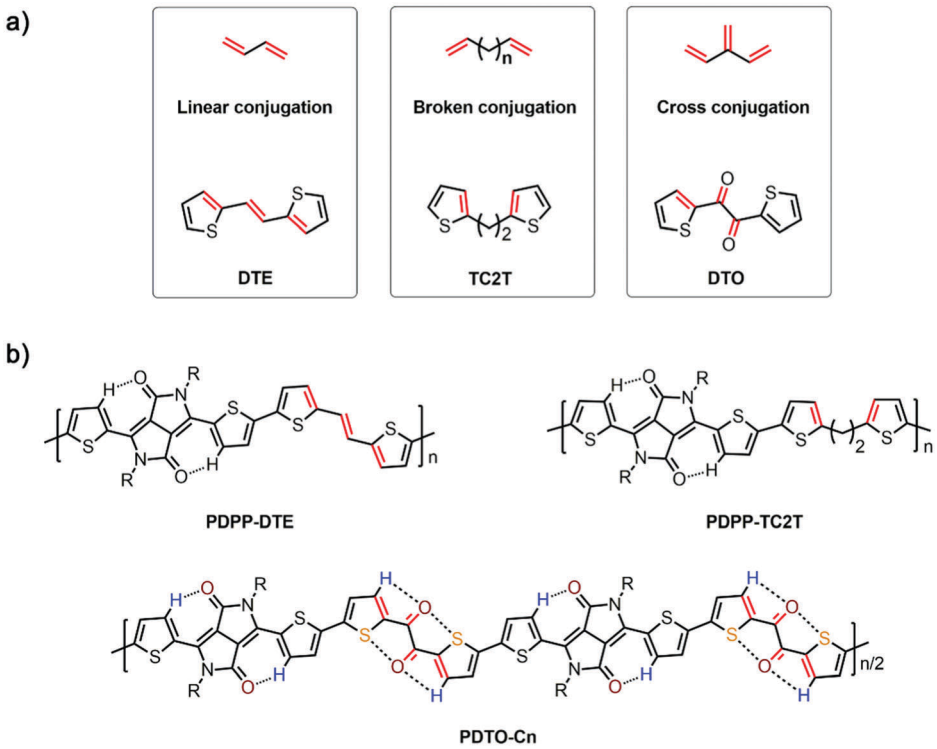

Fig. 1 (a) The chemical structures of broken conjugation, cross-conjugation and linear conjugation using vinyl compounds as examples, and selected thiophene-based units, DTE, TC2T and DTO with three conjugation patterns aforementioned. (b) The chemical structure of the DPP-based alternating polymers, PDPP-DTE and PDPP-TC2T, and a schematic representation of the non-covalent S···O and O···H–C conformational locks in the cross-conjugated DTO-based alternating polymers.

low charge carrier mobilities.[18] It is worthwhile to point out that a cross-conjugated system is distinct from its broken-conjugated counterpart, despite the similarity in their representation as two adjacent single bonds in the conduction path.[19] The single bonds in the former system are still part of a conjugated path whereas the single bonds in the latter system are not. This difference has a significant impact on the change carrier transport characteristics: intra-chain transport may be eliminated in a broken-conjugated system, whereas partially hampered in cross-conjugated systems. Generally speaking, a cross-conjugated system owns a special electronic structure and property in comparison with the other conjugation patterns.

Among the existing design strategies, a reduction in the backbone conformation twists is of prime importance because highly planar π-conjugated backbones are thought to be beneficial for obtaining enlarged overlapping areas between π-orbitals and can enhance the charge carrier mobility.[20,21] Moreover, the planarity of the π-conjugated backbones also has a great influence on the molecular packing, energy levels and crystallinity, which all are also closely related to charge carrier transport in solid state.[22,23] In order to acquire a planar backbone conformation, Facchetti and Marks *et al.* introduced S···O non-covalent intramolecular interactions to the polymer backbones and put forward the concept of "conformational locks" in 2012.[24] Non-covalent intramolecular interactions, acting as conformational locks, can promote the planarity of π-conjugated backbones by limiting the free rotation of the C–C single bonds. Several other research works have also proved that non-covalent conformational locks have widespread influence over the charge transport behaviour of semiconducting polymers.[25,26] Thus, purposefully introducing new planar constructing units with (or with the potential of forming) conformational locks can be considered as an efficient approach in developing high-performance organic semiconductors.

In this work, we have studied cross-conjugated alternating polymers and use them as the active layer of OFET devices, aiming to provide insight into molecular aggregation and charge transport from the aspect of materials design. We have synthesized two DTO-based alternating polymers, namely **PDTO-C1** and **PDTO-C3**, as the basis for our investigation, in which DTO with weak intramolecular S···O and C–H···O interactions was firstly used as a building block to construct polymeric materials (Fig. 1a). The presence of these intramolecular interactions is helpful for obtaining a planar backbone conformation, thus forming a close and ordered packing polymeric thin film. For obtaining a better comparison, two other dithienothiophene (DPP)-based polymers, **PDPP-DTE** (R = 2-decyltridecyl) with a linearly π-conjugated system and **PDPP-TC2T** (R = 4-decyltridecyl) with conjugation-break spacers, are also supplied in Fig. 1b.[18] The PDTO-C1 and PDTO-C3 polymers show high thermal stability (>380 °C) and broad absorption spectra (~900 nm). The OFET devices based on the PDTO-C1 and PDTO-C3 thin films exhibit p-type charge transport characteristic with the highest mobility of 0.22 $cm^2 V^{-1} s^{-1}$ for PDTO-C1, and 0.54 $cm^2 V^{-1} s^{-1}$ for

Published on 09 September 2016. Downloaded by Synchrotron Radiation Library on 11/09/2017 07:30:03.

PDTO-C3. Thin film microstructure investigations indicate that the PDTO-C1 and PDTO-C3 thin films have highly-ordered lamellar packing with π–π stacking distances of 3.58 and 3.50 Å, respectively. The research results demonstrate that by incorporating cross-conjugation to alter their optoelectronic properties provides us an additional design tactic for developing organic semiconductors.

Results and discussion

Synthesis and characterization

The synthetic routes of DTO-based monomers and polymers are shown in Scheme 1. 2-Bromothiophene **1** was firstly converted to the Grignard reagent in dry THF, followed by a cross-coupling reaction with oxalyl chloride in the presence of CuBr and LiBr to give 1,2-di(thiophen-2-yl)ethane-1,2-dione, **2** in high yield.[27] Under weak alkaline conditions, intermediate **2** was brominated using Br_2 to afford the desired monomer **3**.[28] Thiophene-flanked DPP, **4a** and **4b**, reacted with lithium diisopropylamide and was then quenched with 2-isopropoxy-4,4,5,5-tetramethyl-1,3,2-dioxaborolane at 0 °C. After simple precipitation in cooled CH_2Cl_2/acetone, the pure DPP-diboronic esters **5a** and **5b** were obtained as red solids.[29] PDTO-C1 and PDTO-C3 were synthesized according to a modified Suzuki–Miyaura cross-coupling method using $Pd_2(dba)_3$ and P(*o*-tol)$_3$ as the catalyst and ligand, respectively.[8a] The low-molecular-weight oligomers of the crude polymeric materials and noble metal residue were removed by Soxhlet extraction using methanol, acetone and hexane as the eluents, successively. The residual solids were extracted with *o*-dichlorobenzene and precipitated again from methanol to give the desired polymeric materials in high yield. Both polymers are soluble in hot chlorinated solvents such as chlorobenzene and *o*-dichlorobenzene. To obtain a better comparison, a PDPP-TC2T sample was also synthesized according to a reported method (Scheme S1, ESI†).[18b] The PDPP-DTE sample was synthesized based on a literature procedure.[8a] The cross-conjugated polymers were characterized by high-temperature ^{1}H NMR and gel permeation chromatography (GPC) with polystyrene as a standard and 1,2,4-trichlorobenzene as the eluent. The number-average molecular weight (M_n) and polydispersity index (PDI) were found to be 19.8 kDa and 2.32 for PDTO-C1, 22.4 kDa and 2.48 for PDTO-C3, respectively (Table 1). Thermogravimetric analysis (TGA) showed the decomposition temperatures (T_{dec}) with 5% weight loss for PDTO-C1 and PDTO-C3 were 380 and 391 °C, respectively (Fig. S1, ESI†). In addition, no transition was detected from the respective differential scanning calorimetry (DSC) characterization for the two polymers, during the scan from 50 to 250 °C at a rate of 10 °C min^{-1} under a flow of nitrogen.

The crystal structure of dibromo-DTO

A single crystal of dibromo-DTO **3** suitable for X-ray crystallography was prepared by slow diffusion of CH_2Cl_2 solution layered with methanol at room temperature. As shown in Fig. 2, the single crystal belongs to an orthorhombic system with a space group $P2_12_12_1$ (X-ray crystallographic data, see Table S1, ESI†). In the crystal, dibromo-DTO assumes a planar molecular conformation and two kinds of S···O distances of 2.708 and 2.778 Å are observed. Both the S···O distances are apparently smaller than 3.32 Å of the sum of the Van der Waal radii.[30] It is interesting that both C–H···O distances of 2.664 and 2.695 Å are also slightly smaller than the corresponding sum of the Van der Waal radii. These findings imply that weak non-covalent intramolecular

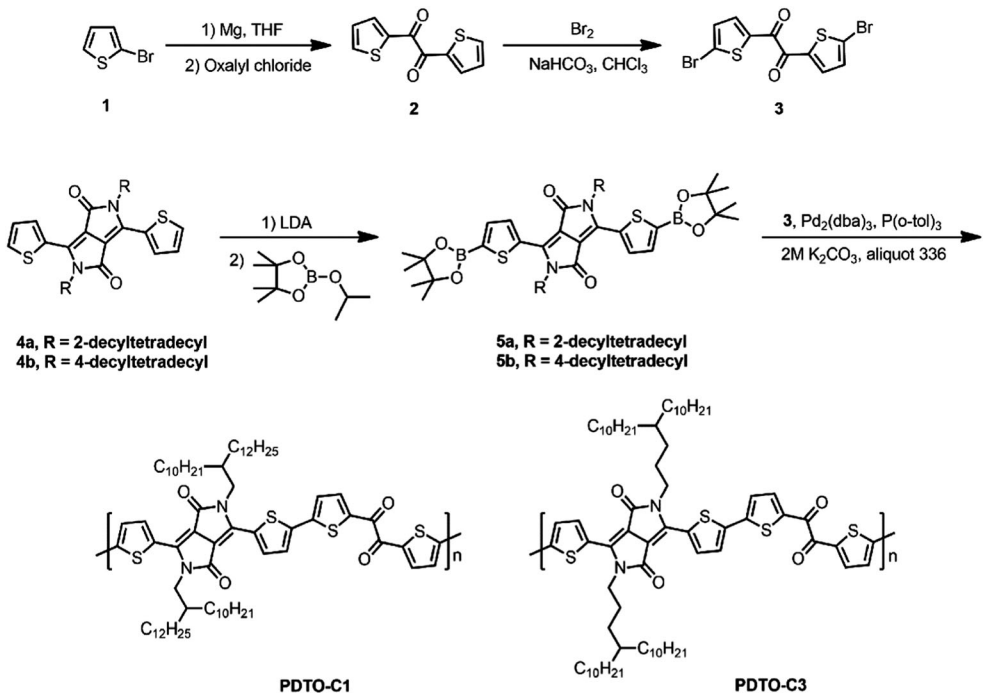

Scheme 1 The synthetic routes used to prepare the DTO-based monomer and the alternating polymers PDTO-C1 and PDTO-C3.

 This journal is © The Royal Society of Chemistry 2016

Published on 09 September 2016. Downloaded by Synchrotron Radiation Library on 11/09/2017 07:30:03.

Table 1 The molecular weights and thermal, optical and electrochemical properties of PDTO-C1 and PDTO-C3

Polymer	M_n/M_w[a] (kDa)	PDI[a]	T_{dec}[b] (°C)	λ_{max} (nm)	E_g^{opt}[e] (eV)	E_{onset}^{ox}[f] (V)	E_{onset}^{red}[f] (V)	HOMO[f] (eV)	LUMO[f] (eV)
PDTO-C1	36.5/22.5	1.62	380	756[c]/734[d]	1.38	1.13	−0.76	−5.53	−3.64
PDTO-C3	49.7/28.4	1.75	391	750[c]/726[d]	1.38	1.15	−0.73	−5.55	−3.67

[a] Determined by GPC at 150 °C. [b] Measured by TGA. [c] In chlorobenzene solution. [d] Thin films. [e] Calculated from the absorption edges of the thin films ($E_g^{opt} = 1240/\lambda_{abs,onset}$). [f] Determined by CV.

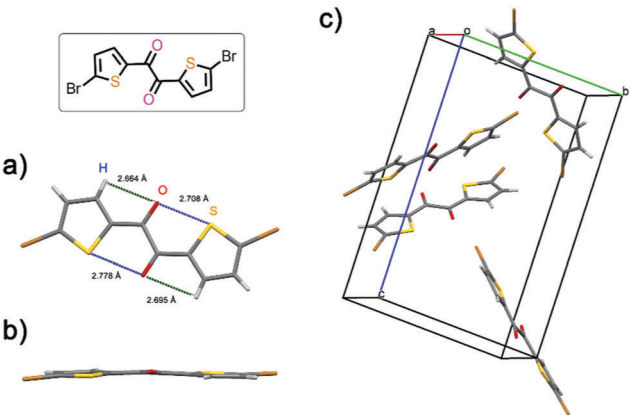

Fig. 2 A packing diagram of the single-crystal X-ray structure of dibromo-DTO, **3** with 50% probability ellipsoids. (a) Side view (S···O, 2.708/2.778 Å, C–H···O, 2.664/2.695 Å). (b) Top view. (c) Stacking pattern.

S···O and C–H···O interactions exist in the DTO unit. These non-covalent interactions, acting as conformational locks, can promote planarity in the polymeric conjugated backbone.[24] Planar π-conjugated backbones are beneficial for obtaining a small π–π stacking distance and close molecular packing as aforementioned. Also, when incorporated to the polymeric π-conjugated backbones, the sp^2-oxygen atoms of the carbonyl groups may endow the resulting polymers with additional intermolecular interactions, thus affording distinct molecular aggregations or microstructures in the solid state, eventually leading to different device performance.[31] The X-ray crystallographic data suggest that the DTO unit can be adopted as a cross-conjugated building block for constructing semiconducting polymers.

Optical properties

The absorption spectra of PDTO-C1 and PDTO-C3 in dilute chlorobenzene are displayed in Fig. 3a. Both polymers show typical dual absorption bands. The high-energy absorption bands, ranging from 300 to 540 nm with peaks at around 460 nm, are associated with the π–π* transition, while the low energy bands, ranging from 540 to 920 nm with peaks at *ca.* 750 nm, are attributed to intramolecular charge transfer (ICT) between the donor and acceptor units.[32] Thin film absorption measurements of the two polymers were measured by spin-coating thin films onto quartz substrates using a chlorobenzene solution (Fig. 3b). When compared to those observed in dilute solutions, the low energy absorption bands of the PDTO-C1 and PDTO-C3 thin films become broader and have blue-shifts of 30 and 16 nm, respectively. The differences are thought to originate from molecular aggregation related to enhanced π–π stacking and the fact that the molecular aggregations amplify their vibronic signals (and relative intensities). Moreover, the absorption maxima of the two cross-conjugated polymers (both in solution and thin film) are both blue-shifted in comparison with the linearly conjugated polymer, PDPP-DTE (*ca.* 800 nm, thin film) and red-shifted to the broken-conjugated polymer, PDPP-TC2T (*ca.* 630 nm, thin film).[18] The different absorption behaviours of the polymers with DTE, TC2T and DTO units are attributed to the different nature of linear conjugation, broken conjugation and cross-conjugation. Different to those in the other two samples, cross-conjugation does not hamper but reduces the electronic communication between the D and A units in the polymers conjugated backbone. From the point of view of electron-donating strength, the weaker electron-donating ability of DTO than DTE unit could be interpreted as one reason for the blue-shifted absorption spectra of the two DTO-based polymers when compared to that of PDPP-DTE. The optical band gaps of PDTO-C1 and PDTO-C3 were estimated to be 1.38 eV based on the absorption edges of their films at *ca.* 900 nm.

Electrochemical properties

The electrochemical properties of both polymers were evaluated by cyclic voltammetry (CV). As shown in Fig. S2 (ESI†), the onset

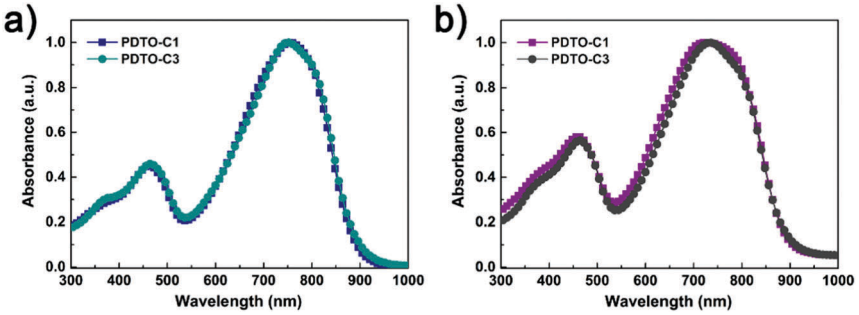

Fig. 3 The UV-vis-NIR absorption spectra of PDTO-C1 and PDTO-C3 in (a) chlorobenzene solution and (b) as thin films.

Published on 09 September 2016. Downloaded by Synchrotron Radiation Library on 11/09/2017 07:30:03.

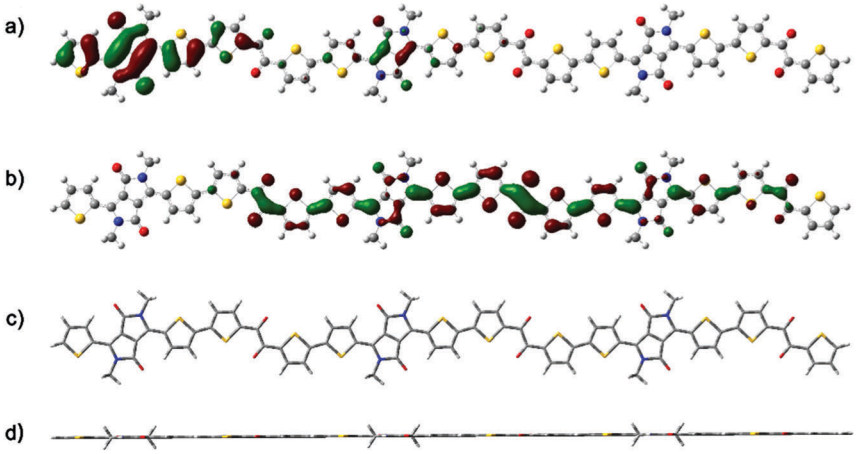

Fig. 4 The molecular orbital amplitude plots and optimized molecular structure of the DTO-based polymer (in trimer) (B3LYP/6-31G*). (a) HOMO, (b) LUMO, (c) side view and (d) top-view of the molecular structure.

oxidation potentials (E^{ox}_{onset}) of PDTO-C1 and PDTO-C3 are 1.13 and 1.15 V *versus* Ag/AgCl, respectively. The HOMO energy levels were estimated to be −5.53 eV for PDTO-C1 and −5.55 eV for PDTO-C3, calculated according to the equation, $E_{HOMO} = -(4.4 + E^{ox}_{onset})$ eV.[33] The deep HOMO energy levels with respect to the vacuum level is beneficial for oxidatively stable devices. Meanwhile, the onset reduction potentials (E^{red}_{onset}) of PDTO-C1 and PDTO-C3 are −0.76 and −0.73 V *versus* Ag/AgCl, respectively, based on which their LUMO energy levels were estimated to be −3.64 and −3.67 eV, respectively, according to the equation, $E_{LUMO} = -(4.4 + E^{red}_{onset})$ eV. The corresponding electrochemical parameters are collected in Table 1. The HOMO energy levels match well with the work function (5.1 eV) of a bare Au electrode, indicating that holes can be injected from a bare Au electrode to the thin films of the DTO-based alternating polymers. To gain more insight into the cross-conjugated system, DFT calculations were performed at the B3LYP/6-31G* level of theory using the Gaussian 03, Revision C. 02 package.[34] Fig. 4 presents the HOMO and LUMO orbital amplitude, and the optimized molecular structure of the DTO-based polymers (in trimer). As shown in the figure, this kind of cross-conjugated polymer possess an almost planar backbone conformation. The computational study also reveals that the HOMOs of the two polymers are localized on the DPP core, whereas the LUMOs are partly delocalized along the polymer chains.

Field-effect transistor fabrication and measurements

The charge transport properties of both polymers were investigated by fabricating FET devices with a bottom-gate/bottom-contact (BGBC) configuration. The polymer thin films were fabricated on a octadecyltrichlorosilane (OTS)-modified Si/SiO_2 substrate with source–drain electrodes by spin-coating a polymer solution in *o*-dichlorobenzene. The fabrication, annealing and measuring processes are all performed under ambient conditions (R_H = 15–20%). Details of the fabrication of the devices are included in the experimental section. The average mobilities were calculated from the transfer characteristics of more than 20 devices in the saturation region (V_{DS} = −100 V). Fig. 5 and Fig. S3 (ESI†) display the typical transfer and output characteristics of the transistor devices based on the PDTO-C3 thin film annealed at 120 °C and the PDTO-C1 thin film annealed at 140 °C for 5 min, respectively. Both polymers exhibit p-type charge transport characteristics. The highest mobility of 0.54 $cm^2\ V^{-1}\ s^{-1}$ (average mobility: 0.36 $cm^2\ V^{-1}\ s^{-1}$) was achieved from PDTO-C3, whereas PDTO-C1 exhibited a mobility of 0.22 $cm^2\ V^{-1}\ s^{-1}$ (average mobility: 0.18 $cm^2\ V^{-1}\ s^{-1}$) (Table 2). The device performances of the thin-film FET devices were heavy affected by the thermal annealing treatments. For the as-spun thin films, the mobility was 0.028 $cm^2\ V^{-1}\ s^{-1}$ (average mobility: 0.02 $cm^2\ V^{-1}\ s^{-1}$) for PDTO-C1, and 0.10 $cm^2\ V^{-1}\ s^{-1}$ (average mobility: 0.08 $cm^2\ V^{-1}\ s^{-1}$) for PDTO-C3. For the thin films annealed at 100 °C for 5 min, the mobilities of PDTO-C1 and PDTO-C3 elevated to 0.095 (average mobility: 0.08 $cm^2\ V^{-1}\ s^{-1}$) and 0.40 $cm^2\ V^{-1}\ s^{-1}$ (average mobility: 0.28 $cm^2\ V^{-1}\ s^{-1}$), respectively. After 5 min of an annealing process at 140 °C for PDTO-C1 and at 120 °C for PDTO-C3, the two polymers exhibited their highest mobilities. The device performance of the OFET based on the PDTO-C1 and PDTO-C3 thin films annealed at other temperatures are collected in Table S2 (ESI†).

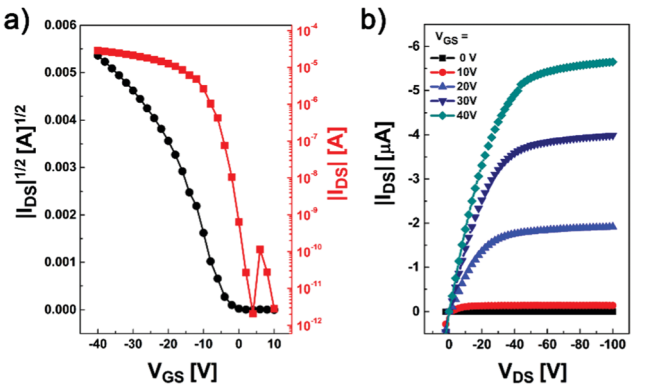

Fig. 5 The typical transfer and output characteristics of the FET devices based on PDTO-C3.

 This journal is © The Royal Society of Chemistry 2016

Published on 09 September 2016. Downloaded by Synchrotron Radiation Library on 11/09/2017 07:30:03.

Table 2 The performance parameters of the PFETs based on PDTO-C1 and PDTO-C3

Polymer	T_{an}[a] (°C)	μ (cm^2 V^{-1} s^{-1})	I_{on}/I_{off}	V_T (V)	d–d (Å)	π–π (Å)
PDTO-C1	25	0.02[b] (0.028)[c]	$>10^4$	5 to −5		
	140	0.18 (0.22)	$>10^6$	−5 to −10	22.4	3.58
PDTO-C3	25	0.08 (0.10)	$>10^4$	−5 to −10		
	120	0.36 (0.54)	$>10^6$	0 to −10	24.5	3.50

[a] Annealing temperature. [b] Average mobility. [c] The highest mobility.

The enhanced charge transport properties at elevated annealing temperatures were attributed to the fact that a suitable thermal annealing treatment is helpful for effective molecular self-assembly in the thin film as observed in other polymer materials.[8,9] It is vital to note that the mobility value of PDTO-C1 was lower than 4.9 cm^2 V^{-1} s^{-1} of PDPP-DTE and the mobility value of PDTO-C3 was much higher than 0.0034 cm^2 V^{-1} s^{-1} of PDPP-TC2T (Fig. S4, ESI†). The comparison roughly reflects the difference between the charge transport properties of the three polymers: the charge carrier mobility of linearly conjugated polymers increases by about two order of magnitude from the broken-conjugated polymer and cross-conjugated polymer. In addition, the highly planar backbone conformation, partially promoted by the S···O and C–H···O conformational locks of the DTO-based polymers, may also have a positive influence on obtaining promising charge transport properties.

Thin film microstructural characterization

To obtain a good understanding of the influence of cross-conjugation, we performed tapping mode atomic force microscopy (AFM) and two-dimensional grazing-incidence X-ray diffraction (2D-GIXRD) experiments to investigate the molecular packing and morphologies of the polymer thin-film samples cast on the OTS-treated Si/SiO_2 substrates. Fig. 6 shows the AFM height images of the PDTO-C1 and PDTO-C3 thin films before and after the annealing treatment. The as-spun films of the two polymers show amorphous morphologies with small crystalline domains. After annealing at the optimal temperature, both the PDTO-C1 and PDTO-C3 thin films exhibit enhanced crystalline morphologies. The annealed PDTO-C1 thin film possesses a uniform morphology with small crystalline fibrillar intercalating networks. Nevertheless, minute grain boundaries also emerge. The annealed PDTO-C3 thin film shows a continuous and slightly rough morphology with apparent crystalline zones, which are likely a result of the enhanced intermolecular π–π interactions. The continuous morphology can avoid the trapping of charge carrier and is helpful for charge carrier transport as demonstrated in several high-performance DPP-based linearly conjugated polymer semiconductors.[8]

The 2D-GIXRD patterns of the PDTO-C1 and PDTO-C3 thin films are shown in Fig. 7. Both as-spun polymer thin films display lamellar textures as judged from the presence of the (h00) Bragg peaks in out-of-plane orientations, in which

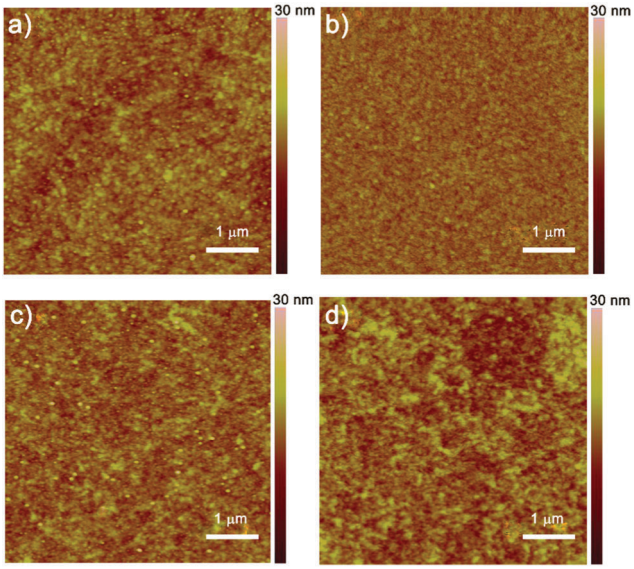

Fig. 6 The tapping mode AFM height images of the DTO-based polymers thin films. The as-spun thin film of (a) PDTO-C1 and (c) PDTO-C3. The annealed thin film of (b) PDTO-C1 at 140 °C and (d) PDTO-C3 at 120 °C. All images are 5 μm × 5 μm in size.

strong (100), (200) and (300) Bragg peaks are observed. After annealing at the respective optimal temperature, even (400) Bragg peaks appear in the 2D-GIXRD patterns of both polymer thin films. The observations imply that the annealed thin films have more orderly molecular packing when compared to their as-spun thin films. Based on the q_z (2.80 and 2.56 nm^{-1}) of the (100) diffraction, the d–d spacing distance was estimated to be 22.4 Å for PDTO-C1 and 24.5 Å for PDTO-C3. The (010) diffraction peaks of the annealed thin films corresponding to π–π stacking are observed in the in-plane (q_{xy}) orientation, whereas no apparent (010) peak appears in the out-plane (q_z) orientation. The findings suggest the two cross-conjugated polymers adopt edge-on molecular packing mode orientated to the OTS-modified Si/SiO_2 substrate. On the basis of the q_{xy} values (17.5 and 17.9 nm^{-1}) of the (010) peak, the π–π stacking distances of the PDTO-C1 and PDTO-C3 thin films were estimated to be 3.58 and 3.50 Å, respectively. The π–π stacking distance of PDTO-C3 was smaller than *ca.* 3.70 Å of PDPP-DTE, implying that the cross-conjugated system exhibits enhanced intermolecular interactions in comparison with its linearly conjugated counterpart.[8a] In addition, the 2D-GIXRD patterns in combination with the AFM images, indicate that the annealed PDTO-C3 thin film has better crystallinity, more dense and orderly molecular arrangement than the counterpart of PDTO-C1. We can ascribe the difference to the more planar backbone conformation of PDTO-C3 than that of PDTO-C1, which was caused by different type of alkyl chains.[35] The thin film microstructure analyses help explain why PDTO-C3 exhibits higher charge mobility than PDTO-C1. On balance, the highly planar cross-conjugated polymers with S···O and C–H···O conformational locks can also form attractive crystalline, dense thin films with

Published on 09 September 2016. Downloaded by Synchrotron Radiation Library on 11/09/2017 07:30:03.

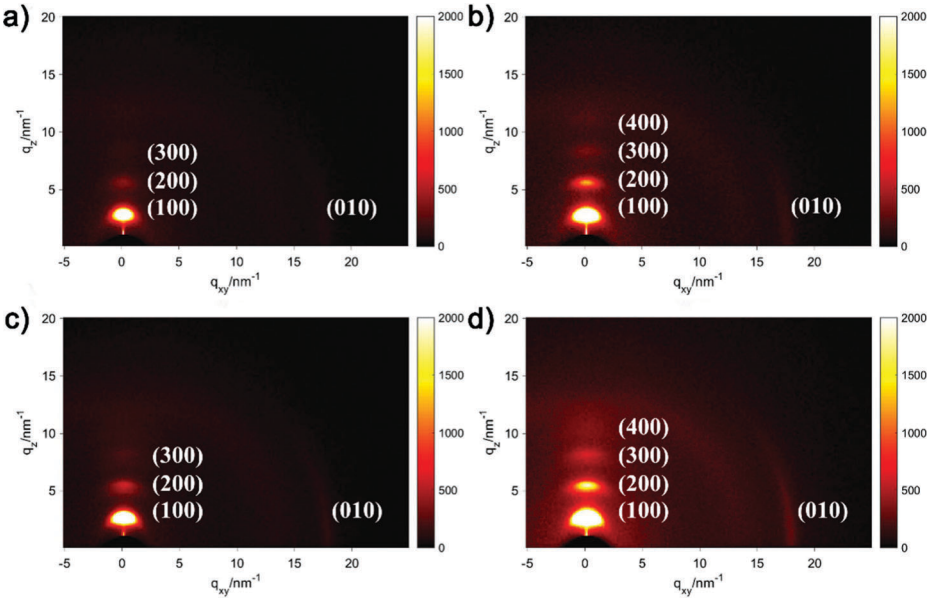

Fig. 7 The 2D-GIXRD patterns of the DTO-based polymers thin films. The as-spun thin film of (a) PDTO-C1 and (c) PDTO-C3. The annealed thin film of (b) PDTO-C1 at 140 °C and (d) PDTO-C3 at 120 °C.

ordered molecular packing as broken-conjugated and linearly conjugated polymers do.

Conclusions

To sum up, we have synthesized two cross-conjugated alternating polymers with multiple conformation locks and investigated their charge transport properties by fabricating OFET devices. The existing non-covalent S···O and C–H···O intramolecular interactions of the DTO unit combined with the C–H···O conformational locks offered by the thiophene-flanked DPP units are beneficial for obtaining a planar polymeric conjugated backbone conformation, which is confirmed by theoretical calculation results. Both polymers display broad UV-vis-NIR absorption spectra. Their absorption spectra (both in solution and in thin film) exhibit a slight blue-shift or a large red-shift in comparison with those of the corresponding linearly conjugated polymer PDPP-DTE and broken-conjugated polymer PDPP-TC2T, respectively. The two highly planar cross-conjugated polymers exhibit promising charge transport properties with the highest mobility of 0.54 cm^2 V^{-1} s^{-1}, which is an order of magnitude higher than that of the broken-conjugated sample. The moderate mobilities can be attributed to the partially blocked electronic communication between donor and acceptor units in the cross-conjugated polymer backbone. However, the AFM and 2D-GIXRD investigations showed that the two cross-conjugated polymers formed attractive crystalline, dense thin films with highly-ordered lamellar packing with π–π stacking distances down to 3.50 Å. The above results suggest that incorporating cross-conjugation can effectively alter the optoelectronic properties of polymer semiconductors, affording an additional design tactic for developing new organic semiconductors.

Experimental section

Material and measurements

All starting materials and catalysts were purchased from commercial sources and used as received if not specified otherwise. Dry tetrahydrofuran (THF) was prepared by distilling over sodium wire/benzophenone under nitrogen. $CHCl_3$ was purified by refluxing over CaH_2 followed by distillation under an inert atmosphere. 1,2-Di(thiophen-2-yl)ethane-1,2-dione (**2**), 1,2-bis(5-bromothiophen-2-yl)ethane-1,2-dione (**3**), thiophene-flanked DPPs (**4**) and the corresponding diboronic esters (**5**) were synthesized according to the synthetic methods reported in the literature.[26,28,29] All air- and water-sensitive reactions were performed under an inert atmosphere. The chemical structures of the intermediates and target molecules were characterized by ^{1}H NMR and ^{13}C NMR spectrocopy on a Bruker Fourier 300 NMR spectrometer and referenced to TMS (0 ppm) or $CDCl_3$ 77 ppm. High resolution mass spectrometry (HRMS) was performed on Bruker APEXII or 9.4T Solarix FT-ICR mass spectrometers. X-ray crystallographic data were collected on a Bruker Smart CCD diffractometer. The structures were resolved by the direct method and refined by full-matrix least-squares on F^2 using the SHELXL-97 program. The polymeric materials were characterized by elemental analysis on a CARLO ERBA 1106 Elemental Analyser. High temperature gel permeation chromatography (GPC) was carried out at 150 °C on a Polymer Labs PL 220 system using 1,2,4-trichlorobenzene as the eluent and polystyrene as the standard. TGA measurements were carried out on a Perkin–Elmer series 7 thermal analysis system under a flow of nitrogen at a heating rate of 10 °C min^{-1}. The absorption spectra were recorded on a Hitachi U-3010 spectrophotometer. Cyclic voltammetry (CV) curves were collected on an electrochemistry workstation at room temperature with a conventional three-electrode configuration in dry acetonitrile containing 0.1 M $(n\text{-Bu})_4NPF_6$ using Platinum stick

 This journal is © The Royal Society of Chemistry 2016

Published on 09 September 2016. Downloaded by Synchrotron Radiation Library on 11/09/2017 07:30:03.

electrode, Ag/AgCl electrode and Platinum wire as working electrode, reference electrode and counter electrode, respectively. The thin film morphology was studied using a Digital Instruments Nanoscope V atomic force microscope operated in tapping mode. 2D-GIXD experiments were performed at a constant incidence angle of 0.2°.

Synthesis of 1,2-di(thiophen-2′-yl)ethane-1,2-dione (2)

To a stirred suspension of CuBr (4.3 g, 30.0 mmol) in dry THF (80 mL) was added dropwise a solution of anhydrous LiBr (5.2 g, 60.0 mmol) in THF (60 mL). The resulting mixture was stirred at the room temperature for 30 min and then cooled at 0 °C. A 1.0 M freshly prepared solution of 2-thienylmagnesium bromide in THF (30.0 mL, 30.0 mmol) and soon afterwards oxalyl chloride (1.2 mL, 12.0 mmol) in THF (20 mL) were quickly added to the stirred solution. The mixture was stirred at 0 °C for 15 min, quenched with saturated aqueous solution of ammonium chloride and extracted with ethyl acetate. The combined organic extract was washed with brine, water and then dried over anhydrous Na_2SO_4. The solvent was removed by rotary evaporation and the residue was purified by silica gel column chromatography using petroleum ether as the eluent affording the desired product as a slight yellow solid (2.45 g, 92%). ^{1}H NMR (300 MHz, $CDCl_3$, δ): 8.08–8.06 (m, 2H), 7.85–7.83 (m, 2H), 7.22–7.19 (m, 2H). ^{13}C NMR (75 MHz, $CDCl_3$, δ): 182.4, 138.6, 137.4, 137.2, 128.6. HRMS: calcd for $[C_{10}H_6O_2S_2]^+$: 221.9809; found: 221.9812.

Synthesis of 1,2-bis(5′-bromothiophen-2′-yl)ethane-1,2-dione (3)

To a 100 mL round-bottom flask containing 1,2-di(thiophen-2-yl)-ethane-1,2-dione **2** (2.0 g, 9.9 mmol) were added $NaHCO_3$ (3.4 g, 40 mmol) and $CHCl_3$ (40 mL). After the suspension was cooled to 0 °C, bromine (2.0 mL, 40 mmol) was added dropwise. Then, the reaction mixture was heated at reflux and stirred for 4 h, then allowed to cool to room temperature, poured into water, extracted with $CHCl_3$ and dried over $MgSO_4$. The solvent was evaporated under reduced pressure and the resulting solid residue was purified by silica gel chromatography using petrolether/dichloromethane as the eluent and subsequent recrystallization from dichloromethane/methanol affording the title compound as yellow needles (2.2 g, 58%). ^{1}H NMR (300 MHz, $CDCl_3$, δ): 7.90 (d, J = 4.2 Hz, 2H), 7.19 (d, J = 4.2 Hz, 2H). ^{13}C NMR (75 MHz, $CDCl_3$, δ): 179.3, 138.4, 137.7, 131.7, 128.1. HRMS: calcd for $[C_{10}H_4Br_2O_2S_2]^+$: 379.7999; found: 379.7994.

General procedures for the DPP-based diboronic esters 5

A solution of thiophene-flanked DPP **4a** or **4b** (1.0 mmol) and 2-isopropoxy-4,4,5,5-tetramethyl-1,3,2-dioxaborolane (0.60 mL, 3.0 mmol) in dry THF (20 mL) was cooled to −25 °C and lithium diisopropylamide (1.2 mL, 2.0 M in heptane, 2.4 mmol) was added dropwise. The reaction was stirred under nitrogen at 0 °C for 1 h. A saturated aqueous solution of ammonium chloride (10 mL) was added, the resulting mixture was extracted with dichloromethane and dried over $MgSO_4$. After removal of the solvent under reduced pressure, the solid residue was dissolved in dichloromethane and poured into cold acetone. After filtration, the resulting filter cake was washed with cold acetone and dried under vacuum affording the title compound as a red powder.

5a. (845 mg, 69%). ^{1}H NMR (300 MHz, $CDCl_3$, δ): 8.91 (d, J = 3.9 Hz, 2H), 7.71 (d, J = 3.9 Hz, 2H), 4.96 (d, J = 7.5 Hz, 4H), 1.89 (br, 2H), 1.37 (s, 24H), 1.21 (br, 80H), 0.89 (m, 12H). ^{13}C NMR (75 MHz, $CDCl_3$, δ): 161.8, 140.5, 137.7, 136.1, 135.7, 1088, 84.6, 46.3, 37.8, 31.9, 31.3, 30.0, 29.7, 29.66, 29.59, 29.36, 26.35, 24.8, 22.7, 14.1. HRMS: calcd for $[C_{74}H_{126}B_2N_2O_6S_2]^+$: 1225.9338; found: 1225.9332.

5b. (796 mg, 65%). ^{1}H NMR (300 MHz, $CDCl_3$, δ): 9.02 (d, J = 3.9 Hz, 2H), 7.71 (d, J = 3.9 Hz, 2H), 4.11 (d, J = 7.5 Hz, 4H), 1.69 (br, 4H), 1.37 (s, 24H), 1.23–1.21 (br, 78H), 0.89 (m, 12H). ^{13}C NMR (75 MHz, $CDCl_3$, δ): 161.4, 140.0, 137.9, 136.3, 135.6, 108.5, 84.6, 42.5, 37.14, 33.5, 31.9, 30.5, 30.1, 29.72, 29.67, 29.64, 29.36, 27.1, 26.6, 24.8, 22.7, 14.1. HRMS: calcd for $[C_{74}H_{126}B_2N_2O_6S_2]^+$: 1225.9338; found: 1225.9324.

General synthetic and purification procedure for PDTO-C1 and PDTO-C3

$Pd_2(dba)_3$ (6 mg) and P(*o*-tol)$_3$ (17 mg) were added quickly to an argon bubbled mixture of DPP-diboronic ester **5a** or **5b** (0.20 mmol) and dibromo-DTO **3** (0.20 mmol), 2 M aqueous K_2CO_3 solution (2 mL), 2 drops of Aliquat 336 and toluene (15 mL). The mixture was stirred at 90 °C for 3 d under an argon atomsphere. Then, phenyl boronic acid was added and the resulting solution was stirred for an additional 4 h, followed by the addition of a few drops of bromobenzene and stirred overnight. The crude polymer was precipitated in methanol (200 mL) containing concentrated hydrochloric acid (2 mL) and subjected to Soxhlet extraction for 2 d in methanol, acetone and hexane in order to remove the low-molecular-weight oligomers of the resultant polymers and catalytic impurities. The solid residue was extracted with *o*-dichlorobenzene and precipitated again from methanol, filtered, washed with methanol and dried under vacuum at room temperature to give the desired polymeric material.

PDTO-C1. (205 mg, 85%). ^{1}H NMR (300 MHz, $C_2D_2Cl_4$, δ): 9.02–8.10 (br, 8H), 5.22–5.09 (br, 4H) 3.18–1.43 (br, 94H). GPC: M_n = 19.8 kDa, M_w = 46.1 kDa, PDI = 2.32. Elemental anal. calcd for $C_{72}H_{108}N_2O_4S_4$: C 72.43; H 9.12, N 2.35; found: C 73.22, H 9.32, N 2.13.

PDTO-C3. (209 mg, 88%). ^{1}H NMR (300 MHz, $C_2D_2Cl_4$, δ): 9.13–8.09 (br, 8H), 4.88–4.63 (br, 4H), 3.09–1.29 (br, 94). GPC: M_n = 22.4 kDa, M_w = 55.5 kDa, PDI = 2.48. Elemental anal. calcd for $C_{72}H_{108}N_2O_4S_4$: C 72.43; H 9.12, N 2.35; found: C 72.87, H 9.29, N 2.08.

X-ray crystallography

X-ray crystallographic data were collected on a Bruker Smart CCD diffractometer using graphite-monochromated Mo Kα radiation (λ = 0.71073 Å). The data were collected at 173 K using ω scan in the θ range of 3.596 to 27.480°. A total of 4648 reflections were measured, of which 2548 were independent reflections [$R_{(int)}$ = 0.0264]. The structure was resolved by the direct method and refined by full-matrix least-squares on F^2 using the SHELXL-97 program. All non-hydrogen atoms were refined anisotropically and all hydrogen atoms were placed using AFIX instructions. Crystallographic data for single crystal of dibromo-DTO **3**: $C_{10}H_4Br_2O_2S_2$; FM = 380.07; crystal size

Published on 09 September 2016. Downloaded by Synchrotron Radiation Library on 11/09/2017 07:30:03.

$0.69 \times 0.18 \times 0.1$ mm^3; orthorhombic; $P2_12_12_1$; a = 5.7908(6) Å; b = 11.3325(13) Å; c = 17.3880(19) Å; $\alpha = 90°$; $\beta = 90°$; $\gamma = 90°$; Z = 4; $\rho_{calculated}$ = 2.212 g cm^{-3}. The refinement was converged to $R_1 = 0.0277$ for $I > 2\sigma(I)$, $R_1 = 0.0571$, w$R_2 = 0.1254$, GOF = 1.069 for all data. CCDC-1400329.

General procedures for OFETs fabrication and measurements

The BGBC field-effect transistor devices were fabricated using a heavily doped Si wafer with 300 nm of SiO_2 layer as the gate electrode and gate dielectric, respectively. The source-drain electrodes (gold/titanium, 30 nm/5 nm) were prepared *via* a photolithography technique with channel widths of 1400 μm. The silica substrates were cleaned using ultrasonication in acetone, deionized water and ethanol, and then treated with octadecyltrichlorosilane (OTS), after which an OTS self-assembled monolayer formed on the surface of silica substrates. Thin films (*ca.* 30 nm) of the polymers were deposited on the OTS-treated substrate by spin-coating using a polymer solution (4 mg mL^{-1}) in *o*-dichlorobenzene, prepared by dissolving the polymer in *o*-dichlorobenzene and stirring at 120 °C for 30 min. The optimized rotation speed was 2500 rpm. The resulting thin films were optionally thermal annealed at selected temperatures for 5 min in air. A Keithley 4200 SCS semiconductor parameter analyser on a probe stage was employed to evaluate the device performance under ambient conditions. The carrier mobility, μ, was calculated from the data in the saturated regime according to the following equation:

$$I_{DS} = \left(\frac{W}{2L}\right) C_i \mu (V_G - V_T)^2$$

where I_{DS} denotes the saturation drain current, W/L is the channel width/length, C_i is the capacitance per unit area of the gate dielectric layer, and V_G and V_T are the gate voltage and threshold voltage, respectively. The channel lengths (L) and channel width (W) of our FET devices were 50 and 1400 μm, respectively.

Acknowledgements

This work was financially supported by the National Natural Science Foundation of China (21474116, 51473021, and 51233006) and the Strategic Priority Research Program of the Chinese Academy of Sciences (XDB12030100), The GIXRD tests were carried out at the BL16B1 Station of Shanghai Synchrotron Radiation Facility (SSRF), 1W1A station of Beijing Synchrotron Radiation Facility (BSRF) and 23A1 Station of National Synchrotron Radiation Research Centre (NSRRC, Taiwan). The authors gratefully thank the assistance of scientists from the stations during the experiments.

Notes and references

1 J. H. Burroughes, D. D. C. Bradley, A. R. Brown, R. N. Marks, K. Mackay, R. H. Friend, P. L. Burn and A. B. Holmes, *Nature*, 1990, **347**, 539.
2 A. Donat-Bouillud, I. Levesque, Y. Tao, M. D'Iorio, S. Beaupré, P. Blondin, M. Ranger, J. Bouchard and M. Leclerc, *Chem. Mater.*, 2000, **12**, 1931–1936.
3 X. L. Yang, G. J. Zhou and W.-Y. Wong, *J. Mater. Chem. C*, 2014, **2**, 1760–1778.
4 (*a*) I. Kang, H. J. Yun, D. S. Chung, S. K. Kwon and Y. H. Kim, *J. Am. Chem. Soc.*, 2013, **135**, 14896–14899; (*b*) Y. Gao, X. J. Zhang, H. K. Tian, J. D. Zhang, D. H. Yan, Y. H. Geng and F. S. Wang, *Adv. Mater.*, 2014, **27**, 6753–6759.
5 H.-J. Yun, S.-J. Kang, Y. Xu, S. O. Kim, Y.-H. Kim, Y.-Y. Noh and S.-K. Kwon, *Adv. Mater.*, 2014, **26**, 7300–7307.
6 (*a*) B. Sun, W. Hong, Z. Q. Yan, H. Aziz and Y. N. Li, *Adv. Mater.*, 2014, **26**, 2636–2642; (*b*) T. Lei, J.-H. Dou, X.-Y. Cao, J.-Y. Wang and J. Pei, *J. Am. Chem. Soc.*, 2013, **135**, 12168–12171.
7 (*a*) P. Sonar, J. J. Chang, Z. G. Shi, E. Gann, J. Li, J. S. Wu and C. R. McNeilld, *J. Mater. Chem. C*, 2015, **3**, 9299–9305; (*b*) G. W. van Pruissen, E. A. Pidko, M. M. Wienk and R. A. Janssen, *J. Mater. Chem. C*, 2014, **2**, 731–735.
8 (*a*) H. J. Chen, Y. L. Guo, G. Yu, Y. Zhao, J. Zhang, D. Gao, H. T. Liu and Y. Q. Liu, *Adv. Mater.*, 2012, **24**, 4618–4622; (*b*) J. Li, Y. Zhao, H. S. Tan, Y. L. Guo, C.-A. Di, G. Yu, Y. Q. Liu, M. Lin, S. H. Lim, Y. Zhou, H. Su and B. S. Ong, *Sci. Rep.*, 2012, **2**, 754.
9 (*a*) C. J. Brabec, S. Gowrisanker, J. J. Halls, D. Laird, S. Jia and S. P. Williams, *Adv. Mater.*, 2010, **22**, 3839–3856; (*b*) X. W. Zhan and D. B. Zhu, *Polym. Chem.*, 2010, **1**, 409–419.
10 (*a*) W. C. Zhao, D. P. Qian, S. Q. Zhang, S. S. Li, O. Inganäs, F. Gao and J. H. Hou, *Adv. Mater.*, 2016, **28**, 4734–4739; (*b*) S. H. Liao, H. J. Jhuo, P. N. Yeh, Y. S. Cheng, Y. L. Li, Y. H. Lee, S. Sharma and S. A. Chen, *Sci. Rep.*, 2014, **4**, 6813.
11 (*a*) Y. Z. Lin, Q. He, F. W. Zhao, L. J. Huo, J. J. Mai, X. H. Lu, C.-J. Su, T. F. Li, J. Y. Wang, J. S. Zhu, Y. M. Sun, C. R. Wang and X. W. Zhan, *J. Am. Chem. Soc.*, 2016, **138**, 2973–2976; (*b*) Y. Z. Lin, F. W. Zhao, Q. He, L. J. Huo, Y. Wu, T. C. Parker, W. Ma, Y. M. Sun, C. R. Wang, D. B. Zhu, A. J. Heeger, S. R. Marder and X. W. Zhan, *J. Am. Chem. Soc.*, 2016, **138**, 4955–4961.
12 (*a*) E. G. Wang, Z. F. Ma, K. Vandewal, P. Henriksson, O. Inganäs, F. L. Zhang and R. A. Andersson, *J. Am. Chem. Soc.*, 2011, **133**, 14244–14247; (*b*) J.-H. Kim, J. B. Park, I. H. Jung, S. C. Yoon, J. Kwakc and D.-H. Hwang, *J. Mater. Chem. C*, 2015, **3**, 4250–4253; (*c*) R. G. Brandt, W. Yue, T. R. Andersen, T. T. Larsen-Olsen, M. Hinge, E. Bundgaard, F. C. Krebsc and D. H. Yu, *J. Mater. Chem. C*, 2015, **3**, 1633–1639.
13 (*a*) C. L. Wang, H. L. Dong, W. P. Hu, Y. Q. Liu and D. B. Zhu, *Chem. Rev.*, 2012, **112**, 2208–2267; (*b*) W. F. Zhang, Y. Q. Liu and G. Yu, *Adv. Mater.*, 2014, **26**, 6898–6904.
14 (*a*) Z. R. Yi, S. Wang and Y. Q. Liu, *Adv. Mater.*, 2015, **27**, 3589; (*b*) T. Lei, J.-Y. Wang and J. Pei, *Acc. Chem. Res.*, 2014, **47**, 1117–1126.
15 (*a*) M. Gholami and R. R. Tykwinski, *Chem. Rev.*, 2006, **106**, 4997–5027; (*b*) A. J. Zucchero, P. L. McGrier and U. H. Bunz, *Acc. Chem. Res.*, 2009, **43**, 397–408.
16 (*a*) D. Venkateshvaran, M. Nikolka, A. Sadhanala, V. Lemaur, M. Zelazny, M. Kepa, M. Hurhangee, A. J. Kronemeijer, V. Pecunia, I. Nasrallah, I. Romanov, K. Broch, I. McCulloch, D. Emin, Y. Olivier, J. Cornil, D. Beljonne and H. Sirringhaus, *Nature*, 2014, **515**, 384–388; (*b*) L. P. Wang, X. D. Xie, S. W. Shi,

 This journal is © The Royal Society of Chemistry 2016

Published on 09 September 2016. Downloaded by Synchrotron Radiation Library on 11/09/2017 07:30:03.

K. L. Shi, Z. P. Mao, W. F. Zhang, H. Q. Wang and G. Yu, *Polymer*, 2015, **68**, 302–307.

17 (*a*) K.-J. Baeg, M. Caironi and Y.-Y. Noh, *Adv. Mater.*, 2013, **25**, 4210–4244; (*b*) J. Y. Huang, Z. P. Mao, Z. H. Chen, D. Gao, C. Y. Wei, W. F. Zhang and G. Yu, *Chem. Mater.*, 2016, **28**, 2209–2218.

18 (*a*) Y. Zhao, X. Zhao, M. Roders, G. Qu, Y. Diao, A. L. Ayzner and J. G. Mei, *Chem. Mater.*, 2015, **27**, 7164–7170; (*b*) X. K. Zhao, Y. Zhao, Q. Ge, K. Butrouna, Y. Diao, K. R. Graham and J. G. Mei, *Macromolecules*, 2016, **49**, 2601–2608.

19 G. C. Solomon, D. Q. Andrews, R. H. Goldsmith, T. Hansen, M. R. Wasielewski, R. P. Van Duyne and M. A. Ratner, *J. Am. Chem. Soc.*, 2008, **130**, 17301–17308.

20 B. Nketia-Yawson, H. S. Lee, D. Seo, Y. Yoon, W. T. Park, K. Kwak, H. J. Son, B. Kim and Y. Y. Noh, *Adv. Mater.*, 2015, **27**, 3045–3052.

21 (*a*) J. E. Coughlin, A. Zhugayevych, R. C. BakusII, T. S. van der Poll, D. C. Welch, S. J. Teat, G. C. Bazan and S. A. Tretiak, *J. Phys. Chem. C*, 2014, **118**, 15610–15623; (*b*) L. Fu, W. Fu, P. Cheng, Z. Xie, C. Fan, M. Shi, J. Ling, J. Hou, X. Zhan and H. Chen, *J. Mater. Chem. A*, 2014, **2**, 6589–6597.

22 J. S. Lee, S. K. Son, S. Song, H. Kim, D. R. Lee, K. Kim, M. J. Ko, D. H. Choi, B. Kim and J. H. Cho, *Chem. Mater.*, 2012, **24**, 1316–1323.

23 W. F. Zhang, N. H. Zheng, C. Y. Wei, J. Y. Huang, D. Gao, K. L. Shi, J. Xu, D. H. Yan, Y. C. Han and G. Yu, *Polym. Chem.*, 2016, **7**, 1413–1421.

24 H. Huang, Z. H. Chen, R. P. Ortiz, C. Newman, H. Usta, S. Lou, J. Youn, Y.-Y. Noh, K.-J. Baeg, L. X. Chen, A. Facchetti and T. J. Marks, *J. Am. Chem. Soc.*, 2012, **134**, 10966–10973.

25 (*a*) S. Yum, T. K. An, X. W. Wang, W. Lee, M. A. Uddin, Y. J. Kim, T. L. Nguyen, S. H. Xu, S. Hwang, Ch. E. Park and H. Y. Woo, *Chem. Mater.*, 2014, **26**, 2147–2154; (*b*) T. Lei, X. Xia, J.-Y. Wang, C.-J. Liu and J. Pei, *J. Am. Chem. Soc.*, 2014, **136**, 2135–2141.

26 (*a*) Z. P. Mao, W. F. Zhang, J. Y. Huang, K. L. Shi, D. Gao, Z. H. Chen and G. Yu, *Polym. Chem.*, 2015, **6**, 6457–6464; (*b*) W. F. Zhang, K. L. Shi, J. Y. Huang, D. Gao, Z. P. Mao, D. Z. Li and G. Yu, *Macromolecules*, 2016, **49**, 2582–2591.

27 F. Babudri, V. Fiandanese, G. Marchese and A. Punzi, *Tetrahedron Lett.*, 1995, **36**, 7305–7308.

28 M. Mastalerz, V. Fischer, C.-Q. Ma, R. A. J. Janssen and P. P. Bäuerle, *Org. Lett.*, 2009, **11**, 4500–4503.

29 (*a*) C. H. Woo, P. M. Beaujuge, T. W. Holcombe, O. P. Lee and J. M. J. Fréchet, *J. Am. Chem. Soc.*, 2010, **132**, 15547–15549; (*b*) D. Cortizo-Lacalle, S. Arumugam, S. E. T. Elmasly, A. L. Kanibolotsky, N. J. Findlay, A. R. Inigo and P. J. Skabara, *J. Mater. Chem.*, 2012, **22**, 11310–11315; (*c*) C. Cheng, C. M. Yu, Y. L. Guo, H. J. Chen, Y. Fang, G. Yu and Y. Q. Liu, *Chem. Commun.*, 2013, **49**, 1998–2000.

30 S. Alvarez, *Dalton Trans.*, 2013, 8617–8636.

31 D. Niedzialek, V. Lemaur, D. Dudenko, J. Shu, M. R. Hansen, J. W. Andreasen, W. Pisula, K. Müllen, J. Cornil and D. Beljonne, *Adv. Mater.*, 2013, **25**, 1939–1947.

32 (*a*) J. Y. Wang, K. L. Shi, Y. Suo, Y. Z. Lin, G. Yu and X. W. Zhan, *J. Mater. Chem. C*, 2016, **4**, 3781–3791; (*b*) J. S. Ha, K. H. Kim and D. H. Choi, *J. Am. Chem. Soc.*, 2011, **133**, 10364–10367.

33 (*a*) W. F. Zhang, K. L. Shi, W. L. Zhou, Z. G. Li, Z. H. Chen, J. Xu, D. H. Yan, Y. C. Han, M. S. Wong, F. H. Li and G. Yu, *Dyes Pigm.*, 2016, **131**, 1–8; (*b*) W. F. Zhang, X. N. Sun, P. F. Xia, G. Yu, M. S. Wong, Y. Q. Liu and D. B. Zhu, *Org. Lett.*, 2012, **14**, 4382–4385.

34 M. J. Frisch, G. W. Trucks, H. B. Schlegel, G. E. Scuseria, M. A. Robb, J. R. Cheeseman, J. A. Montgomery, Jr., T. Vreven, K. N. Kudin, J. C. Burant, J. M. Millam, S. S. Iyengar, J. Tomasi, V. Barone, B. Mennucci, M. Cossi, G. Scalmani, N. Rega, G. A. Petersson, H. Nakatsuji, M. Hada, M. Ehara, K. Toyota, R. Fukuda, J. Hasegawa, M. Ishida, T. Nakajima, Y. Honda, O. Kitao, H. Nakai, M. Klene, X. Li, J. E. Knox, H. P. Hratchian, J. B. Cross, V. Bakken, C. Adamo, J. Jaramillo, R. Gomperts, R. E. Stratmann, O. Yazyev, A. J. Austin, R. Cammi, C. Pomelli, J. W. Ochterski, P. Y. Ayala, K. Morokuma, G. A. Voth, P. Salvador, J. J. Dannenberg, V. G. Zakrzewski, S. Dapprich, A. D. Daniels, M. C. Strain, O. Farkas, D. K. Malick, A. D. Rabuck, K. Raghavachari, J. B. Foresman, J. V. Ortiz, Q. Cui, A. G. Baboul, S. Clifford, J. Cioslowski, B. B. Stefanov, G. Liu, A. Liashenko, P. Piskorz, I. Komaromi, R. L. Martin, D. J. Fox, T. Keith, M. A. AlLaham, C. Y. Peng, A. Nanayakkara, M. Challacombe, P. M. W. Gill, B. Johnson, W. Chen, M. W. Wong, C. Gonzalez and J. A. Pople, *Gaussian 03, Revision C.02*, Gaussian, Inc., Wallingford, CT, 2004.

35 T. Lei, J.-H. Dou and J. Pei, *Adv. Mater.*, 2012, **24**, 6457–6461.